Computer simulation of diffraction contrast images of small dislocation loops in icosahedral quasicrystals

1993 J. Phys.: Condens. Matter 5 2935

(http://iopscience.iop.org/0953-8984/5/18/016)

J. Phys.: Condens. Matter 5 (1993) 2935–2946. Printed in the UK

Computer simulation of diffraction contrast images of small dislocation loops in icosahedral quasicrystals

Z G Wang†‡ and R Wang†§

† Beijing Laboratory of Electron Microscopy, Academia Sinica, PO Box 2724, 100080 Beijing, People's Republic of China

‡ Department of Materials Physics, University of Science and Technology Beijing, 100083 Beijing, People's Republic of China

§ Department of Physics, Wuhan University, 430072 Wuhan, People's Republic of China

Received 8 September 1992, in final form 3 December 1992

Abstract. The strain-field expression of a small dislocation loop (SDL) in an elastically isotropic medium is extended to the case of icosahedral quasicrystals. The diffraction contrast images of SDL are simulated systematically for different experimental and SDL parameters. The main results of the simulation are explained semiquantitatively by the contrast expressions for the SDL deduced by a perturbation treatment.

1. Introduction

Since the discovery of the Al–Mn icosahedral quasicrystal (IQC) (Shechtman *et al* 1984), the defects in quasicrystals (QC) have been extensively studied both theoretically and experimentally. In the framework of either a density-wave description or a unit-cell picture, the theories of elasticity and dislocation defects in QC were proposed and discussed by Levine *et al* (1985), Lubensky and Ramaswamy (1986), Socolar *et al* (1986) and De and Pelcovits (1987). A generalized Volterra process, which implies the insertion or removal of a half-hyperplane in a six-dimensional (6D) hypercubic lattice and subsequent projection into the three-dimensional (3D) physical space, was used to produce a dislocation in an IQC by Bohsung and Trebin (1987), Kleman (1988) and Kleman and Sommers (1991). These theoretical studies demonstrate that, in order to describe a defect in QC, it is necessary to introduce a phason strain field $\boldsymbol{R}_\perp(\boldsymbol{r})$ in addition to the conventional phonon strain field $\boldsymbol{R}_\parallel(\boldsymbol{r})$ in crystals; hence six parameters are needed to index the Burgers vector $\tilde{\boldsymbol{b}}$ of a dislocation. Dislocations in QC have also been observed experimentally either directly in high-resolution electron microscopy (HREM) images (Hiraga 1987) or by means of HREM image processing (Wang *et al* 1987). By using the methods of diffraction contrast analysis and higher-order Laue zone (HOLZ) lines, dislocations, stacking faults and dislocation networks have been analysed (Devaud-Rzepski *et al* 1989, Zhang and Urban 1989, Zhang *et al* 1990, Yan *et al* 1992, Wang *et al* 1993, Yan and Wang 1993, Dai 1993).

Recently, we have observed and studied systematically a small dislocation loop (SDL) in an Al–Mn–Si IQC by the method of diffraction contrast (Wang *et al* 1991). In crystals, for SDL the variations of the contrast image characteristics with different parameters (e.g. the Burgers vector $\boldsymbol{b}$, loop plane normal $\boldsymbol{n}$, depth z_0 of the SDL, foil thickness t, foil normal $\boldsymbol{F}$, electron beam incident direction $\boldsymbol{B}$, diffraction vector $\boldsymbol{g}$ and deviation parameter w)

0953-8984/93/182935+12$07.50

have been investigated in detail by Wilkens and his colleagues (Wilkens and Rühle 1972, Häussermann *et al* 1972, Wilkens and Föll 1978, Wilkens 1978) and Saldin *et al* (1978). According to these results, the type and distribution of SDL in many metals have been identified successfully. In order to deepen our understanding of the characteristics of SDL in QC, in this paper we simulate systematically the diffraction contrast images of SDL in IQC for different parameters. The main results of the simulation are explained semiquantitatively by the contrast expressions for the SDL deduced by a perturbation calculation.

2. Strain field of the small dislocation loop in icosahedral quasicrystals

The ideal and defect-free icosahedral quasilattice can be constructed by projection from a periodic hypercubic lattice $E^{(6)}$ in 6D space $S^{(6)}$ onto 3D physical space $S_{\parallel}^{(3)}$ (our 3D world) in such a way that the projected basis vectors $\{e_{\parallel}^{i}\}$ $(i = 1, \ldots, 6)$ coincide with six icosahedral basis vectors along the six fivefold axes of an icosahedron. Let $\{\tilde{e}^{i}\}$ $(i = 1, \ldots, 6)$ denote the standard orthogonal basis in $S^{(6)}$. The projection can be performed with a projection matrix $\mathbf{P}_{\parallel}$:

$$(e_{\parallel}^{1}, \ldots, e_{\parallel}^{6})^{\mathrm{T}} = \mathbf{P}_{\parallel}(\tilde{e}^{1}, \ldots, \tilde{e}^{6})^{\mathrm{T}} \tag{2.1}$$

where the superscript T means transpose of the matrix. Another projection matrix

$$\mathbf{P}_{\perp} = \mathbf{I} - \mathbf{P}_{\parallel} \tag{2.2}$$

(**I** is a unit matrix) produces a set of projected basis vectors $\{e_{\perp}^{i}\}$ in 3D pseudo-space $S_{\perp}^{(3)}$, which is orthogonal to $S_{\parallel}^{(3)}$:

$$(e_{\perp}^{1}, \ldots, e_{\perp}^{6})^{\mathrm{T}} = \mathbf{P}_{\perp}(\tilde{e}_{1}, \ldots, \tilde{e}_{6})^{\mathrm{T}}. \tag{2.3}$$

So any position vector $\tilde{r}$ in $S^{(6)}$ can be expressed as the direct sum of its two components $r_{\parallel}$ and $r_{\perp}$ respectively in $S_{\parallel}^{(3)}$ and $S_{\perp}^{(3)}$:

$$\tilde{r} = r_{\parallel} \oplus r_{\perp} = \mathbf{P}_{\parallel}(\tilde{r}) \oplus \mathbf{P}_{\perp}(\tilde{r}). \tag{2.4}$$

The icosahedral quasilattice can be obtained by projecting those hyperlattice points with the position vectors $\tilde{r} \in E^{(6)}$ if their orthogonal components $r_{\perp} \in c_{\perp}$, where $c_{\perp}$ is a unit triacontahedron in $S_{\perp}^{(3)}$.

Dislocations in QC are best defined in the high-dimensional space where full periodicity is recovered, and the dislocations can be constructed in the usual way by the Volterra process as singular topological defects characterized by a Burgers vector $\tilde{b}$ of the hyperlattice. Then the arrangement of the defective lattice in our 3D space can be obtained by projection from $E^{(6)}$ to $S_{\parallel}^{(3)}$. If a dislocation is induced into 6D hypercubic lattice $E^{(6)}$, the hyperlattice points will produce a shift from their proper position $\tilde{r}$ to $\tilde{r}' = \tilde{r} + \tilde{R}$. The 6D displacement field $\tilde{R}$ can be written as

$$\tilde{R} = (R_1, R_2, R_3, R_4, R_5, R_6) = \sum_{i=1}^{6} R_i \tilde{e}^{i} \tag{2.5}$$

where R_i $(i = 1, \ldots, 6)$ are six components of $\tilde{R}$ in $S^{(6)}$.

The displacement field $\tilde{R}$ must fulfil an important requirement in order to be consistent with the basic property of IQC of being structurally independent of the actual location of the physical space $S_{\parallel}^{(3)}$ in the 6D space $S^{(6)}$ (local isomorph classes): the displacement field $\tilde{R}$ generated by the dislocation must be invariant by any translation along the pseudo-space $S_{\perp}^{(3)}$, i.e. the displacement field $\tilde{R}$ in 6D space $S^{(6)}$ is a function of the physical space variable $r_{\parallel}$ only. As a consequence,

$$\tilde{R}(r_{\parallel}) = (R_1(r_{\parallel}), R_2(r_{\parallel}), R_3(r_{\parallel}), R_4(r_{\parallel}), R_5(r_{\parallel}), R_6(r_{\parallel})) = \sum_{i=1}^{6} R_i(r_{\parallel})\tilde{e}^i. \tag{2.6}$$

since $\tilde{e}^i = e_{\parallel}^i \oplus e_{\perp}^i$ $(i = 1, \ldots, 6)$ we have

$$\tilde{R}(r_{\parallel}) = \sum_{i=1}^{6} R_i(r_{\parallel})e_{\parallel}^i \oplus \sum_{i=1}^{6} R_i(r_{\parallel})e_{\perp}^i = R_{\parallel}(r_{\parallel}) \oplus R_{\perp}(r_{\parallel}) \tag{2.7}$$

where

$$R_{\parallel}(r_{\parallel}) = \sum_{i=1}^{6} R_i(r_{\parallel})e_{\parallel}^i \tag{2.8}$$

$$R_{\perp}(r_{\parallel}) = \sum_{i=1}^{6} R_i(r_{\parallel})e_{\perp}^i \tag{2.9}$$

are two components of $\tilde{R}(r_{\parallel})$ respectively in physical and perpendicular (pseudo-) spaces. The parallel component $R_{\parallel}(r_{\parallel})$ is responsible for the elastic deformation around the dislocation as in conventional crystals (phonon strain) while the perpendicular component $R_{\perp}(r_{\parallel})$ leads to a local rearrangement of the basic tiles (phason strain) around the dislocation. Therefore, $R_{\parallel}((r_{\parallel})$ and $R_{\perp}(r_{\parallel})$ are spanned with the same span coefficients in two different representations, i.e. in physical space basis $\{e_{\parallel}^i\}$ and pseudo-space basis $\{e_{\perp}^i\}$.

According to Ding (1993), the equilibrium equations for QC expressed by displacements $R_{\parallel}(r_{\parallel})$ and $R_{\perp}(r_{\parallel})$ are

$$C_{ijkl}\partial_j\partial_l R_{\parallel}^k + P_{ijkl}\partial_j\partial_l R_{\perp}^k + f_i = 0 \tag{2.10a}$$

$$K_{ijkl}\partial_j\partial_l R_{\perp}^k + P_{klij}\partial_j\partial_l R_{\parallel}^k + g_i = 0 \tag{2.10b}$$

where C_{ijkl} and K_{ijkl} are elastic tensors corresponding to the phonon and phason strains respectively, P_{ijkl} is the elastic tensor coupling $R_{\parallel}(r_{\parallel})$ to $R_{\perp}(r_{\parallel})$, $R_{\parallel}^k$ and $R_{\perp}^k$ are the kth components of $R_{\parallel}(r_{\parallel})$ and $R_{\perp}(r_{\parallel})$, and f_i (or g_i) is the ith component of the body force per unit volume. By neglecting the coupling term (that is $P_{ijkl} = 0$) equation (2.10a) reduces to the following simpler form

$$C_{ijkl}\partial_j\partial_l R_{\parallel}^k + f_i = 0 \tag{2.11}$$

which is the same as the equilibrium equation of classical elasticity (Hirth and Lothe 1968).

In elastic isotropic crystals, the displacement field $R(r)$ of a SDL is expressed as (Kroupa 1963)

$$R(r) = -\frac{S}{8\pi(1-\nu)}\left(\frac{1-2\nu}{r^3}[(b\cdot r)n + (n\cdot r)b - (n\cdot b)r] + \frac{3}{r^5}(b\cdot r)(n\cdot r)r\right) \tag{2.12}$$

where S is the loop area, r the position vector from the centre of the SDL, n the unit vector normal to the loop plane and ν the Poisson ratio.

It is well known (e.g. Wang and Kuo 1990) that cubic point group 23 is a subgroup of icosahedral point group 235, and crystals with symmetry 23 have three independent elastic constants. Using any fivefold rotation operator in point group 235, we can prove there are only two independent elastic constants for the phonon strain in IQC. Consequently, when neglecting the coupling term the phonon strain field $\boldsymbol{R}_\parallel(\boldsymbol{r}_\parallel)$ of a SDL in IQC has the same expression as the formula (2.12):

$$\boldsymbol{R}_\parallel(\boldsymbol{r}_\parallel) = -\frac{S}{8\pi(1-\nu)}\left(\frac{1-2\nu}{r_\parallel^3}[(\boldsymbol{b}_\parallel\cdot\boldsymbol{r}_\parallel)\boldsymbol{n}_\parallel + (\boldsymbol{n}_\parallel\cdot\boldsymbol{r}_\parallel)\boldsymbol{b}_\parallel - (\boldsymbol{n}_\parallel\cdot\boldsymbol{b}_\parallel)\boldsymbol{r}_\parallel] + \frac{3}{r_\parallel^3}(\boldsymbol{b}_\parallel\cdot\boldsymbol{r}_\parallel)(\boldsymbol{n}_\parallel\cdot\boldsymbol{r}_\parallel)\boldsymbol{r}_\parallel\right) \tag{2.13}$$

where $\boldsymbol{b}_\parallel$ and $\boldsymbol{n}_\parallel$ are the components in the physical space of the Burgers vector $\tilde{\boldsymbol{b}} = \boldsymbol{b}_\parallel \oplus \boldsymbol{b}_\perp$ and unit vector $\tilde{\boldsymbol{n}} = \boldsymbol{n}_\parallel \oplus \boldsymbol{n}_\perp$ of the loop plane normal, respectively, and $\boldsymbol{b}_\perp$ and $\boldsymbol{n}_\perp$ are the corresponding perpendicular components. The exact expression $\boldsymbol{R}_\perp(\boldsymbol{r}_\parallel)$ is unknown. As a first approximation, we may express the vectors $\boldsymbol{n}_\parallel$ and $\boldsymbol{r}_\parallel$ in equation (2.13) by six components

$$\boldsymbol{n}_\parallel = \sum_{i-1}^{6} n_i \boldsymbol{e}_\parallel^i \qquad \boldsymbol{r}_\parallel = \sum_{i=1}^{6} x_i \boldsymbol{e}_\parallel^i. \tag{2.14}$$

Then by using equations (2.7) to (2.9) $\boldsymbol{R}_\perp(\boldsymbol{r}_\parallel)$ may be expressed as

$$\boldsymbol{R}_\perp(\boldsymbol{r}_\parallel) = -\frac{S}{8\pi(1-\nu)}\left(\frac{1-2\nu}{r_\parallel^3}[(\boldsymbol{b}_\parallel\cdot\boldsymbol{r}_\parallel)\boldsymbol{n}_\perp + (\boldsymbol{n}_\parallel\cdot\boldsymbol{r}_\parallel)\boldsymbol{b}_\perp - (\boldsymbol{n}_\parallel\cdot\boldsymbol{b}_\parallel)\boldsymbol{r}_\perp] + \frac{3}{r_\parallel^5}(\boldsymbol{b}_\parallel\cdot\boldsymbol{r}_\parallel)(\boldsymbol{n}_\parallel\cdot\boldsymbol{r}_\parallel)\boldsymbol{r}_\perp\right) \tag{2.15}$$

where

$$\boldsymbol{n}_\perp = \sum_{i=1}^{6} n_i \boldsymbol{e}_\perp^i \qquad \boldsymbol{r}_\perp = \sum_{i=1}^{6} x_i \boldsymbol{e}_\perp^i. \tag{2.16}$$

Obviously the coefficients n_i and x_i in equations (2.14) and (2.16) are not unique, because it is impossible to determine uniquely the six components n_i (or x_i) from a three-component vector $\boldsymbol{n}_\parallel$ (or $\boldsymbol{r}_\parallel$). In the conventional crystals, for a vacancy (or interstitial) SDL we have $\boldsymbol{n}\cdot\boldsymbol{b} > 0$ (or $\boldsymbol{n}\cdot\boldsymbol{b} < 0$). Although a dislocation in IQC cannot be regarded as the insertion or removal of a half-plane of atoms, the effect of contraction (or expansion) in the neighbourhood of a SDL still exists when $\boldsymbol{n}_\parallel\cdot\boldsymbol{b}_\parallel > 0$ (or $\boldsymbol{n}_\parallel\cdot\boldsymbol{b}_\parallel < 0$), just like the case in crystals. So here we still call them 'vacancy' ($\boldsymbol{n}_\parallel\cdot\boldsymbol{b}_\parallel > 0$) or 'interstitial' ($\boldsymbol{n}_\parallel\cdot\boldsymbol{b}_\parallel < 0$) type SDL.

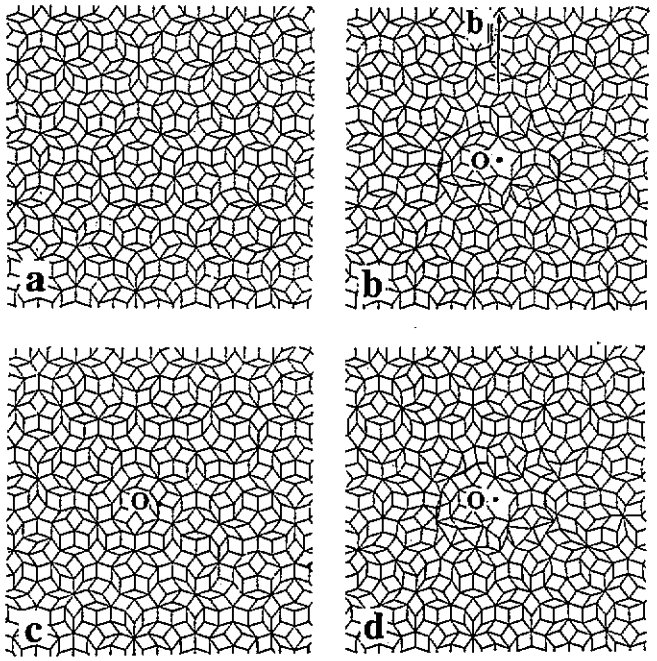

Figure 1. Section–projection diagrams of the IQC perpendicular to a fivefold axis [0 1 0 0 0]: (*a*) perfect IQC; (*b*) IQC containing a SDL at O with $\vec{b} \parallel \vec{n} \parallel$ [1 0 0 1 0 0]; (*c*) only considering the phason strain ($\boldsymbol{R}_{\parallel} = 0$); (*d*) only considering the phonon strain ($\boldsymbol{R}_{\perp} = 0$).

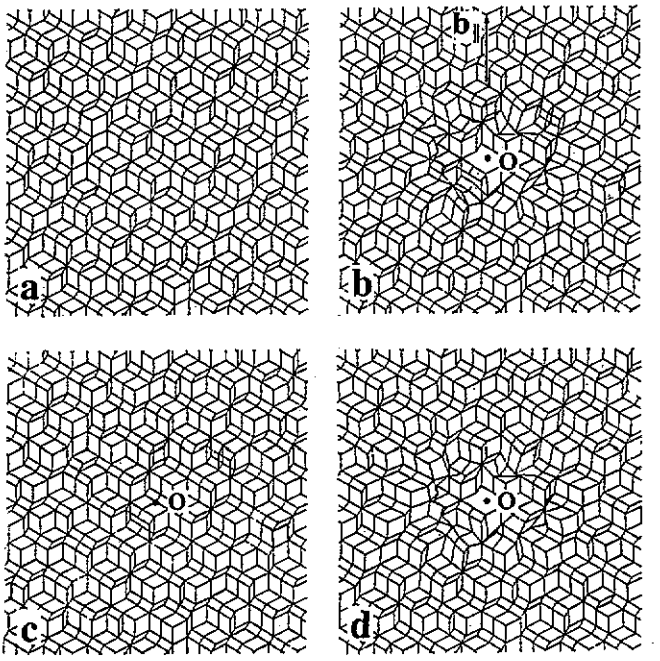

Figure 2. Section–projection diagrams of the IQC perpendicular to a twofold axis [0 0 1 0 $\bar{1}$ 0]: (*a*) perfect IQC; (*b*) IQC containing a SDL at O with $\vec{b} \parallel \vec{n} \parallel$ [1 0 0 1 0 0]; (*c*) only considering the phason strain ($\boldsymbol{R}_{\parallel} = 0$); (*d*) only considering the phonon strain ($\boldsymbol{R}_{\perp} = 0$).

3. Section–projection diagrams of icosahedral quasicrystals containing a small dislocation loop

In order to describe diagrammatically the lattice model of a SDL we provide here several groups of section–projection diagrams of the IQC containing a SDL with $\vec{b} \parallel \vec{n} \parallel$[1 0 0 1 0 0] (vacancy type) according to the method proposed by Katz and Duneau (1986). Figures 1;

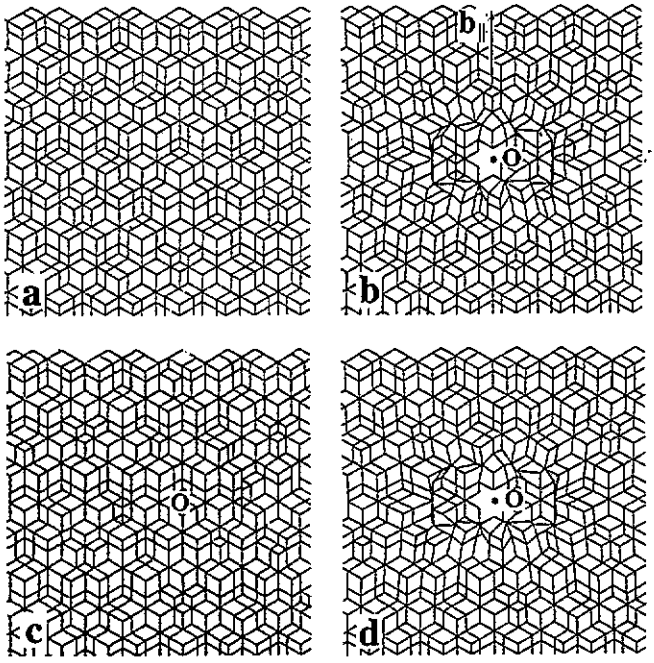

Figure 3. Section–projection diagrams of the IQC perpendicular to a threefold axis $[0\,1\,1\,0\,\bar{1}\,0]$: (*a*) perfect IQC; (*b*) IQC containing a SDL at O with $\tilde{\boldsymbol{b}} \parallel \tilde{\boldsymbol{n}} \parallel [1\,0\,0\,\bar{1}\,0\,0]$; (*c*) only considering the phason strain ($\boldsymbol{R}_\parallel = 0$); (*d*) only considering the phonon strain ($\boldsymbol{R}_\perp = 0$).

2 and 3 are such section diagrams perpendicular to the fivefold axis $[0\,1\,0\,0\,0\,0]$, twofold axis $[0\,0\,1\,0\,\bar{1}\,0]$ and threefold axis $[0\,1\,1\,0\,\bar{1}\,0]$, respectively. Parts (*a*) of these figures are all section diagrams of the perfect icosahedral quasilattice, which appear as perfect five-, two- and threefold generalized Penrose tiling. Parts (*b*) of these figures show the quasilattice sections containing a SDL centred at the point O. In order to show the phason strain and phonon strain fields separately, we provide the contribution of the phason strain $\boldsymbol{R}_\perp$ in parts (*c*) and that of the phonon strain $\boldsymbol{R}_\parallel$ in parts (*d*) of these figures. From these figures it is obvious that the phonon displacement field $\boldsymbol{R}_\parallel$ causes the quasilattice points in the neighbourhood of the SDL to shift towards the centre of the SDL mainly along the $\pm\boldsymbol{b}_\parallel$ directions, and the phason strain field $\boldsymbol{R}_\perp$ causes the rearrangement of some quasilattice points. These may be seen more clearly in figure 4, where full lines relate to the generalized Penrose tiling perpendicular to the threefold axis of the perfect icosahedral quasilattice while broken lines show that containing the SDL. The rearrangement of the quasilattice points induces mistakes of the tiling.

4. Simulation of contrast images of small dislocation loops in icosahedral quasicrystals

The dynamical theory of electron diffraction for crystals containing defects can be extended to quasicrystals if the contribution $\boldsymbol{g} \cdot \boldsymbol{R}$ to the phase factor caused by the defects is replaced by $\tilde{\boldsymbol{g}} \cdot \tilde{\boldsymbol{R}}$, where $\tilde{\boldsymbol{g}}$ is a 6D reciprocal vector (Wang and Cheng 1987). In section 2, we have obtained the strain-field expressions (2.13) and (2.15) of a SDL in the IQC; then the diffraction contrast images can be calculated out from the extended Howie–Whelan equations. Noting the uncertainty of the coefficients n_i and x_i we tried to simulate the contrast image by using different n_i and x_i values (Wang and Wang 1992). Our systematic simulation shows that the concrete phason strain expression has very little effect on the simulated contrast images. This result is not a surprise because $\boldsymbol{g}_\perp$ is very small compared with corresponding $\boldsymbol{g}_\parallel$ for strong reflections and hence we have $|\boldsymbol{g}_\perp \cdot \boldsymbol{R}_\perp| \ll |\boldsymbol{g}_\parallel \cdot \boldsymbol{R}_\parallel|$.

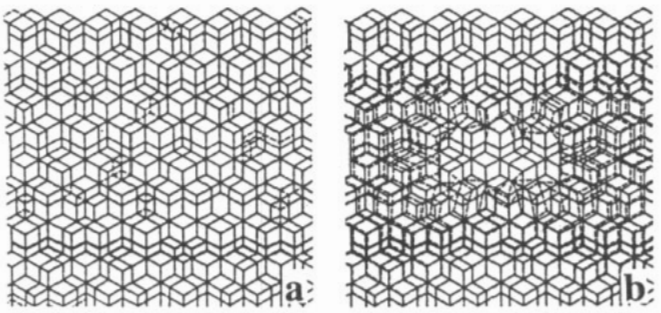

Figure 4. Section–projection diagrams of the IQC perpendicular to the threefold axis $[0\,1\,1\,0\,\bar{1}\,0]$ showing the contributions (broken lines) of (*a*) the phason strain $\boldsymbol{R}_\perp$ and (*b*) the phonon strain $\boldsymbol{R}_\parallel$ of a SDL in IQC (full lines are the generalized Penrose tiling of the perfect IQC).

4.1. Deviation parameter oscillation

The results of our simulation show that a loop with its centre close to one of the foil surfaces appears as a black–white (B–W) contrast under the dynamical two-beam condition. The orientation of the B–W vector $\boldsymbol{l}$ (the vector joining the centre of the black lobe to the centre of the white lobe) is almost independent of the direction of $\tilde{\boldsymbol{g}}$ and lies parallel (or antiparallel) to the Burgers vector $\boldsymbol{b}_\parallel$ or to its projection onto the image plane (i.e. the plane perpendicular to the electron beam direction $\boldsymbol{B}$). With the variation of the deviation parameter w, the contrast of the SDL changes as shown in figure 5. Figure 5(*a*) shows the simulated bright-field (BF) contrast images of the SDL near the top surface, with the following parameters: $\tilde{\boldsymbol{b}} \| \tilde{\boldsymbol{n}} \| [1\,0\,0\,1\,0\,0]$, $\boldsymbol{B} \| [1\,0\,0\,0\,0\,1]$, $\tilde{\boldsymbol{F}} \| [3\,2\,0\,0\,0\,1]$, $t = 4.5\xi_g$ with ξ_g being the extinction distance, $z_0 = 0.25\xi_g$ and $w = -3.5$, -1.5, 0.0, 1.25 and 3.5 respectively from the left-hand side to the right-hand side. It shows an oscillation of B–W contrast with w, i.e. the direction of B–W vector $\boldsymbol{l}$ reveals reversal with w increasing from negative value ($= -3.5$) to positive value ($= 3.5$). Figure 5(*b*) shows the simulated BF images of the SDL near the bottom surface ($z_0 = 4.25\xi_g$) corresponding to figure 5(*a*). It is obvious that the B–W contrast from the SDL close to the bottom surface is reversed compared with that close to the top surface (figure 5(*a*)). Figure 5(*c*) shows experimental BF images observed in the annealed Al–Mn–Si IQC, which are in good agreement with the theoretically simulated one shown in figure 5(*b*).

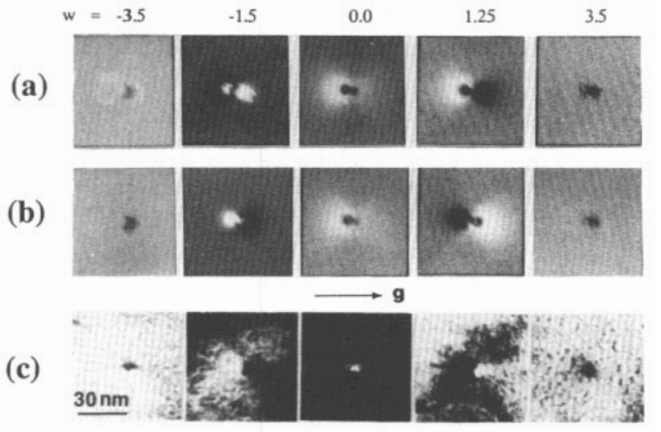

Figure 5. The variation of BF contrast images of a SDL in IQC with the deviation parameter w: (*a*) the simulated images of the SDL near the top surface; (*b*) the simulated images of the SDL near the bottom surface; (*c*) the experimental images observed in annealed Al–Mn–Si IQC.

4.2. Depth oscillation

There also exists a depth oscillation effect of the B–W contrast. Figure 6(*a*) shows the variation of BF image contrast of a vacancy SDL with its depth z_0 at different deviation parameters w. When $w = 0$, the depth oscillation phenomenon is the same as that in the case of crystals, revealed by Wilkens (1978). The regions close to the foil surface are divided into layers L1, L2 and L3 with a thickness of $0.3\xi_g$, $0.45\xi_g$ and $0.5\xi_g$, respectively. Near the boundaries of these layers the image appears as a dot. It becomes a B–W lobe in the middle of each layer and the sense of the lobe reverses from one layer to the neighbouring layer. For loops in the middle of the foil, the contrast appears as a black speckle of irregular shape. When $w = \pm 1.5$, the regions close to the foil surface are divided into six layers with a layer thickness of about $0.25\xi_g$ for each layer, and the depth oscillations extend deeper into the foil. In this case, the oscillation periodicity (the layer thickness) becomes smaller than that when $w = 0$.

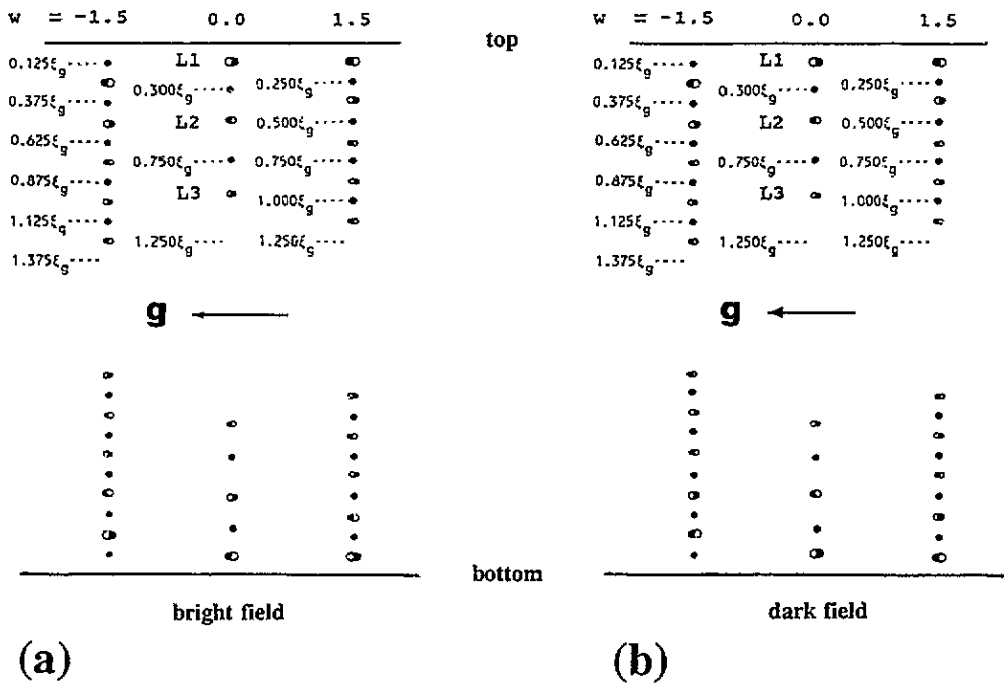

Figure 6. Schematic plot of the depth oscillation for different deviation parameters w of the B–W contrast figures from SDL of vacancy type in IQC; the contrast figures are drawn at those depth positions at which the loop centres were assumed: (*a*) the BF contrast figures; (*b*) the DF contrast figures.

4.3. Symmetry properties

Figure 6(*b*) shows the calculated dark-field (DF) images of the SDL at different depths and with different deviation parameters w. By comparing figures 6(*a*) and 6(*b*) it is apparent that the BF and DF images are similar when the SDL is close to the top surface while they are complementary when the SDL is close to the bottom surface. Moreover, the DF

contrast is nearly symmetrical about the middle plane of the foil while the BF contrast is antisymmetrical. Such behaviour coincides with the well known symmetry properties of diffraction contrast (Hirsch *et al* 1965).

4.4. Effect of the directions of $b_{\parallel}$ and $n_{\parallel}$

For convenience of identifying the directions of the Burgers vectors $b_{\parallel}$ and the habit plane normal $n_{\parallel}$ of the SDL by means of the diffraction contrast technique, we have carried out a series of simulations by varying the directions of the Burgers vector $b_{\parallel}$ and the habit plane normal $n_{\parallel}$ of the SDL with respect to the directions of the incident beam B and the diffraction vector $g_{\parallel}$. The results are shown in figure 7 where each BF contrast image lies at the position of the stereographic projection of the Burgers vector $b_{\parallel}$, which is taken to be parallel to $n_{\parallel}$. If the angle between $b_{\parallel}(n_{\parallel})$ and $g_{\parallel}$ is not large ($\leqslant 45°$), the contrast image consists of one black and one white lobe whose B–W vector l lies parallel (or antiparallel) to the projection of $b_{\parallel}$ onto the image plane. If $b_{\parallel}(n_{\parallel})$ is nearly perpendicular to $g_{\parallel}$ and the angle between $b_{\parallel}(n_{\parallel})$ and B is large enough, the contrast image is of 'butterfly' shape consisting of three pairs of B–W lobes, in which the B–W lobe parallel (or antiparallel) to $g_{\parallel}$ is weaker and narrower than the other two pairs of B–W lobes. When the angle between $b_{\parallel}(n_{\parallel})$ and $g_{\parallel}$ is about 50–80° and the angle between $b_{\parallel}(n_{\parallel})$ and B is large enough, the contrast image appears as two pairs of B–W lobes. The main B–W lobe has its l direction nearly parallel (or antiparallel) to the projection of the $b_{\parallel}(n_{\parallel})$ direction onto the imaging plane while the weaker B–W lobe has its l nearly parallel (or antiparallel) to the $g_{\parallel}$ direction. When the angle between $b_{\parallel}(n_{\parallel})$ and B is small, complicated contrast images result.

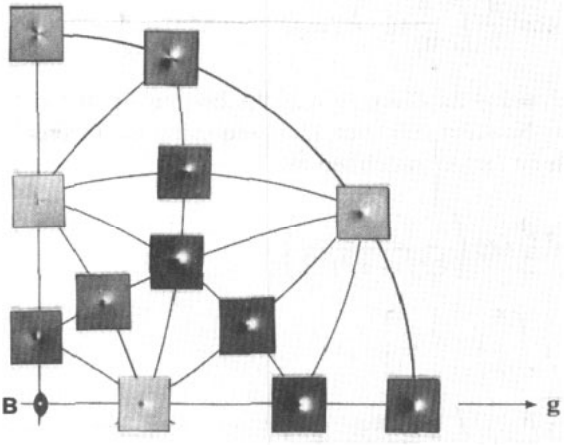

Figure 7. The contrast variation with the direction of $b_{\parallel}$ and $n_{\parallel}$ of SDL.

5. Analytical expression of the diffraction contrast of the small dislocation loop

The analytical calculations of the two-beam dynamical theory for SDL in crystals proposed by Wilkens (1978) and Wang (1983) can only be used for the case of $w = 0$ (dynamical imaging condition). Now we extend these calculations to the case of the kinematical condition ($w \neq 0$) as follows. We start from the equations (11.9) for the modified excitation coefficients $\psi'^{(i)}$ ($i = 1, 2$) given by Hirsch *et al* (1965):

$$\mathrm{d}\psi'^{(1)}/\mathrm{d}z = -2\pi\mathrm{i}(\mathrm{d}/\mathrm{d}z)(\tilde{\boldsymbol{g}} \cdot \tilde{\boldsymbol{R}}) \sin(\beta/2) \cos(\beta/2) \exp(2\pi\mathrm{i}\Delta kz)\psi'^{(2)}$$

$$\mathrm{d}\psi'^{(2)}/\mathrm{d}z = -2\pi\mathrm{i}(\mathrm{d}/\mathrm{d}z)(\tilde{\boldsymbol{g}} \cdot \tilde{\boldsymbol{R}}) \sin(\beta/2) \cos(\beta/2) \exp(-2\pi\mathrm{i}\Delta kz)\psi'^{(1)} \quad (5.1)$$

where here and afterwards β, w and s are deviation parameters, $w = \cot\beta$, $w = s\xi_g$, and

$$\Delta k = (1 + w^2)^{1/2}/\xi_g + i/[\xi_g'(1 + w^2)^{1/2}] + (1/z)\tilde{g} \cdot \tilde{R} \cos\beta. \tag{5.2}$$

ξ_g' is the anomalous absorption distance and usually we have $\xi_g \ll \xi_g'$.

The 'width' Δ of the strain field $\tilde{R}$ of a SDL is very small ($\Delta \ll \xi_g$). If the depth z_0 of the SDL lies not too close to the surfaces of the foil specimen ($z_0 > \Delta$) and we do not consider the contrast at positions near the centre of the SDL, then we have

$$\tilde{g} \cdot \tilde{R} \ll 1 \qquad (d/dz)\tilde{g} \cdot \tilde{R} \ll 1/\Delta \tag{5.3}$$

and the boundary condition at the top surface:

$$\psi'^{(1)}(0) = \cos(\beta/2) \qquad \psi'^{(2)}(0) = \sin(\beta/2). \tag{5.4}$$

Under the condition (5.3) we can treat equation (5.1) by means of the first-order perturbation calculation that equation (5.1) may be integrated directly by replacing $\psi'^{(1)}$ and $\psi'^{(2)}$ appearing on the right-hand sides by their values at the top surface of the foil (see equation (5.4)):

$$\psi'^{(1)}(t) = \cos\frac{\beta}{2}\left(1 - 2\pi i \sin^2\frac{\beta}{2}\int_0^t \frac{d}{dz}(\tilde{g} \cdot \tilde{R}) \exp(2\pi i \Delta k z)\, dz\right)$$

$$\psi'^{(2)}(t) = \sin\frac{\beta}{2}\left(1 - 2\pi i \cos^2\frac{\beta}{2}\int_0^t \frac{d}{dz}(\tilde{g} \cdot \tilde{R}) \exp(-2\pi i \Delta k z)\, dz\right). \tag{5.5}$$

We introduce a new integral variant $\zeta = z - z_0$. Since $\Delta < z_0$ the integral limits for ζ can be taken as being from $-\infty$ to $+\infty$. Noticing condition (5.3) and using the theorem of integration by parts, equation (5.5) can be further simplified as:

$$\psi'^{(1)}(t) = \cos\frac{\beta}{2}\left[1 - 4\pi^2\frac{(1 + w^2)^{1/2}}{\xi_g}\sin^2\frac{\beta}{2}\exp\left(\frac{-2\pi z_0}{\xi_g'(1 + w^2)^{1/2}}\right)\right.$$
$$\left.\times \exp\left(2\pi i\frac{(1 + w^2)^{1/2}}{\xi_g}z_0\right)\int_{-\infty}^{\infty}\tilde{g} \cdot \tilde{R}\, d\zeta\right]$$

$$\psi'^{(2)}(t) = \sin\frac{\beta}{2}\left[1 + 4\pi^2\frac{(1 + w^2)^{1/2}}{\xi_g}\cos^2\frac{\beta}{2}\exp\left(\frac{2\pi z_0}{\xi_g'(1 + w^2)^{1/2}}\right)\right.$$
$$\left.\times \exp\left(-2\pi i\frac{(1 + w^2)^{1/2}}{\xi_g}z_0\right)\int_{-\infty}^{\infty}\tilde{g} \cdot \tilde{R}\, d\zeta\right]. \tag{5.6}$$

The amplitude of the transmitted wave is proportional to

$$u_0(t) = \Psi'^{(1)}(t)\cos\frac{\beta}{2}\exp\left[-\pi\left(\frac{1}{\xi_0'} - \frac{1}{\xi_g'(1 + w^2)^{1/2}}\right)t\right] + \Psi'^{(2)}(t)\sin\frac{\beta}{2}$$
$$\times \exp\left(2\pi i\frac{(1 + w^2)^{1/2}}{\xi_g}t\right)\exp\left[-\pi\left(\frac{1}{\xi_0'} + \frac{1}{\xi_g'(1 + w^2)^{1/2}}\right)t\right] \tag{5.7}$$

where ξ_0' is the mean absorption distance.

When $w \geqslant 0$ the contribution of the first term in equation (5.7) to $u_0(t)$ in much larger than that of the second term, and hence we obtain the approximate expression for the contrast function c as follows:

$$C_+ = -4\pi^2 \frac{(1+w^2)^{1/2}}{\xi_g} \left(1 - \frac{w}{(1+w^2)^{1/2}}\right) \exp\left(\frac{-2\pi z_0}{\xi_g'(1+w^2)^{1/2}}\right) \times \cos\left[2\pi\left(\frac{(1+w^2)^{1/2}}{\xi_g} z_0\right)\right] \int_{-\infty}^{\infty} \tilde{\boldsymbol{g}} \cdot \tilde{\boldsymbol{R}}\, \mathrm{d}\zeta. \tag{5.8}$$

When $w \leqslant -1.5$ the contribution of the second term in equation (5.7) is larger and we have the contrast function:

$$C_- = 4\pi^2 \frac{(1+w^2)^{1/2}}{\xi_g} \left(1 + \frac{w}{(1+w^2)^{1/2}}\right) \exp\left(\frac{2\pi z_0}{\xi_g'(1+w^2)^{1/2}}\right) \times \cos\left[2\pi\left(\frac{(1+w^2)^{1/2}}{\xi_g} z_0\right)\right] \int_{-\infty}^{\infty} \tilde{\boldsymbol{g}} \cdot \tilde{\boldsymbol{R}}\, \mathrm{d}\zeta. \tag{5.9}$$

6. Discussion

When the deviation parameter $w \simeq 0$ (two-beam dynamical condition), the depth oscillation, the symmetry properties and the effect of the directions of $\boldsymbol{b}_\parallel$ and $\boldsymbol{n}_\parallel$, as described in section 4, are all the same as in the case of crystals; see the review written by Wilkens (1978). In the case of crystals Wilkens (1978) and Wang (1983) explained all these phenomena semiquantitatively by a first-order perturbation treatment of the two-beam dynamical theory. According to this theory the B–W lobe contrast comes from the fact that the value of the inner product $\boldsymbol{g} \cdot \boldsymbol{R}$ reverses when the position vector $\boldsymbol{r}$ reverses. In the case of the IQC the contribution $\boldsymbol{g} \cdot \boldsymbol{R}$ to the phase factor of the theory should be replaced by the 6D inner product $\tilde{\boldsymbol{g}} \cdot \tilde{\boldsymbol{R}} = \boldsymbol{g}_\parallel \cdot \boldsymbol{R}_\parallel \oplus \boldsymbol{g}_\perp \cdot \boldsymbol{R}_\perp$, where $\boldsymbol{g}_\parallel$ is the component of $\tilde{\boldsymbol{g}}$ in 3D parallel space. For strong reflection, $\boldsymbol{g}_\perp$ is very small compared with the corresponding $\boldsymbol{g}_\parallel$, and hence we have $\tilde{\boldsymbol{g}} \cdot \tilde{\boldsymbol{R}} \simeq \boldsymbol{g}_\parallel \cdot \boldsymbol{R}_\parallel$. Consequently, all properties of the contrast images that exist in the SDL in crystals may be extended to the SDL in QC when strong reflections are excited.

For the case of $w \neq 0$, equations (5.8) and (5.9) show that, when $|w|$ increases, the factors $1 - w/(1+w^2)^{1/2}$ in equation (5.8) and $1 + w/(1+w^2)^{1/2}$ in equation (5.9) will decrease, and the contrast of the SDL tends to zero. When $|w| = 1.5$, there is a weaker B–W lobe contrast, which shows also a depth oscillation with a period of $\xi_g/(1+w^2)^{1/2}$. This period is equal to $0.55\xi_g$ when $|w| = 1.5$, which is in good agreement with the simulated results shown in figure 6(*a*) where the depth oscillation period is about $0.5\xi_g$ for $|w| = 1.5$.

Figure 6 shows a phase shift phenomenon of the depth oscillation when $|w| \neq 0$ (i.e. $C \propto \cos[2\pi z_0(1+w^2)^{1/2}/\xi_g - \alpha]$). This effect is not included in equations (5.8) and (5.9) where we only considered the contribution from one of the two Bloch waves.

The deviation parameter oscillation observed experimentally (figure 5(*c*)) and revealed by accurate simulation (figures 5(*a*) and (*b*)) is the consequence of the different depth oscillation periods and different phase shifts for different deviation parameters w.

Acknowledgment

This project was supported by the National Natural Science Foundation of China.

References

Bohsung J and Trebin H-R 1987 *Phys. Rev. Lett.* **58** 2277
Dai M X 1993 *Phil. Mag.* A at press
De P and Pelcovits R A 1987 *Phys. Rev.* B **35** 8609
Devaud-Rzepski J Cornier-Quiquandon M and Gratias D 1989 *Proc. 3rd Int. Conf. on Quasicrystals (Vista Hermosa, Mexico, 1989)* ed M J Yacaman *et al* (Singapore: World Scientific) p 498
Ding D H 1993 private communication
Häussermann F, Rühle M and Wilkens M 1972 *Phys. Status Solidi* b **50** 445
Hiraga K 1987 *Japan J. Appl. Phys* **26** L155
Hirsch P B, Howie A, Nicholson R B, Pashley D W and Whelan M J 1965 *Electron Microsopy of Thin Crystals* (London: Butterworths) pp 259, 291
Hirth J P and Lothe J 1968 *Theory of Dislocations* (New York: McGraw-Hill) p 32
Katz A and Duneau M 1986 *J. Physique* **47** 181
Kleman M 1988 *Proc. Workshop on Quasicrystalline Material (Grenoble, 1988)* ed Ch Janot and J M Dubois (Singapore: World Scientific) p 318
Kleman M and Sommers C 1991 *Acta Metall. Mater* **39** 287
Kroupa F 1963 *Czech. J. Phys.* A **13** 301
Levine D, Lubensky T C, Ostlund S, Ramaswamy S, Steinhardt P J and Toner J 1985 *Phys. Rev. Lett.* **54** 1520
Lubensky T C and Ramaswamy S 1986 *Phys. Rev.* B **33** 7715
Saldin D K, Stathopoulos A Y and Whelan M J 1978 *Electron Diffraction 1927–1977 (Inst. Phys. Conf. Ser. 41)* ed P J Dobson, J B Pendry and C J Humphreys (Bristol: Institute of Physics) p 350
Shechtman D, Blech I A, Gratias D and Cahn J W 1984 *Phys. Rev. Lett.* **53** 1951
Socolar J E S, Lubensky T C and Steinhardt P J 1986 *Phys. Rev.* B **34** 3345
Wang D N, Ishimasa T, Nissen H-U, Hovmöller S and Rhyner J 1987 *Phil. Mag* A **58** 737
Wang R 1983 *J. Chin. Electron Microsc.* **2** (3) 1 (in Chinese)
Wang R and Cheng Y F 1987 *Mater. Sci. Forum* **22–24** 409
Wang R and Kuo K H 1990 *Symmetry Groups in Crystallography* (Beijing: China Science Press) p 133 (in Chinese)
Wang R, Yan Y F and Kuo K H 1993 *J. Non-Cryst. Solids* **153 & 154** 103
Wang Z G and Wang R 1992 *Proc. 5th Asia–Pacific Electron Microscopy Conf.: Electron Microscopy 1 (Beijing, China, 1992)* ed K H Kuo and Z H Zhai (Singapore: World Scientific) p 514
Wang Z G, Wang R and Deng W F 1991 *Phys. Rev. Lett.* **66** 2124
Wilkens M 1978 *Diffraction and Imaging Techniques in Materials Science* ed S Amelinckx, R Gevers and J Van Landuyt (Amsterdam: North-Holland) p 185
Wilkens M and Föll H 1978 *Phys. Status Solidi* a **49** 555
Wilkens M and Rühle M 1972 *Phys. Status Solidi* b **49** 749
Yan Y F and Wang R 1993 *J. Mater. Res* **8** 286
Yan Y F, Wang R and Feng J L 1992 *Phil. Mag. Lett.* **66** 197
Zhang Z and Urban K 1989 *Phil. Mag. Lett.* **60** 97
Zhang Z, Wollgarten M and Urban K 1990 *Phil. Mag. Lett.* **61** 125